Nonlinear Studies - www. nonlinearstudies.com
MESA - www.journalmesa.com

Preprint submitted to Nonlinear Studies / MESA

Fluid Solid Interaction Simulation of CFRP Shell Structure

H. Khawaja[1,⋆],R. Messahel[2],M. Souli[2],E. Al-Bahkali[3],M. Moatamedi[1]

[1]UiT The Arctic University of Norway, Norway.
[2]Université de Lille, France.
[3]King Saud University, KSA.

⋆ *Corresponding Author*: hassan.a.khawaja@uit.no

Abstract. This work attempts to model the dynamic behavior of Carbon Fiber Reinforced Polymer (CFRP) shell structure subjected to water shock wave to improve the results presented in the study by Khawaja et al., 2014. In the previous study, the real physical problem was simplified by decoupling the fluid and the structural phenomena, applying the recorded experimental fluid pressure load to the CFRP shell structure. The current study involves not only structure modeling, as given in the earlier study, but also fluid behavior using the Arbitrary Lagrangian-Eulerian (ALE) method. The focus of this study is to highlight the difference in structural response between uncoupled and coupled Fluid Structure Interaction (FSI) numerical solution, and also to validate the ability of the FSI numerical simulation to solve complex problems, involving the generation and the propagation of water shock waves and their impact on the composite shell structures, using both multi-material ALE (MM-ALE) methods and advanced non-linear Fluid Structure Interaction (FSI) strong coupling algorithms. Results obtained from experiments are compared with numerical simulations using the LS-DYNA® software. The results are found to be in good agreement with the experimental data and are improved by considering the coupling effects, as the mass of the water acts as a viscous damper and reduces the high-frequency oscillations in the structural response.

1 Introduction

Fluid-structure interaction (FSI) has become more and more the focus of computational engineering in recent years. Real-life engineering applications require accurate and consistent numerical modeling that is usually memory and CPU-time consuming. Recently, the increase in computing power and parallel computing has been used to solve complex fluid-structure interaction problems that could not be solved in the past.

Unlike structure-structure contact, fluid-structure contact can generate extremely high mesh distortion, mainly at the fluid-structure interface, where a fluid element may become so distorted that the

2010 **Mathematics Subject Classification** 93B52; 93B51; 93D15; 35B37
Keywords: Fluid-Structure Interaction (FSI), Arbitrary-Lagrangian-Eulerian (ALE), Shock Tube, Carbon Fiber Reinforced Polymer (CFRP)

volume of the element is calculated as negative, which terminates the computation before physical termination time. In order to prevent fluid mesh distortion for fluid-structure application, the fluid is solved using a multi-material ALE (MM-ALE) formulation with fixed mesh[1] and a Lagrangian method with deformable mesh for the structure that is embedded inside the MM-ALE fluid mesh. These overlapping finite element meshes has been co-developed in LS-DYNA® software by the third author of the paper and have been validated for several applications, including multiphase shock tube simulation [2], airbag deployment in the automotive industry [3], the aerospace industry [3], civil engineering [4, 5], the nuclear industry [6, 7] and in bio-mechanics [8, 9].

In this paper, we present the validation of ALE and FSI to solve the dynamic response of CFRP shell structures under a cyclic pressure loading generated by an air-water shock tube. In section 2, the governing equations of the ALE formulation are described, and the advection algorithms used to solve mass, momentum and energy conservation in the multi-material formulation are discussed. Section 3 describes the experimental setup designed to test CFRP shells subjected to water shock waves. The last two sections are devoted to numerical simulation and the validation of ALE formulations, combined with the FSI capabilities of LS-DYNA to solve such complex problems.

2 ALE multi-material formulation and FSI

2.1 ALE multi-material formulation

A brief description of the ALE formulation used in this paper is presented; additional details are given in [1]. To solve fluid-structure interaction problems, a Lagrangian formulation is performed for the structure and an ALE formulation for the fluid materials; where water and air materials can be mixed in the same element, this element is referred to as a mixed element, since it contains two different materials: water and air, as described in Fig. 1. A mixture theory is used to partition the material inside the element and compute the volume weighted stress from the constitutive model of each material, as described in [10]. Let Ω_t^{ALE} be an arbitrary domain of boundary Γ_t^{ALE}, we define the injective function

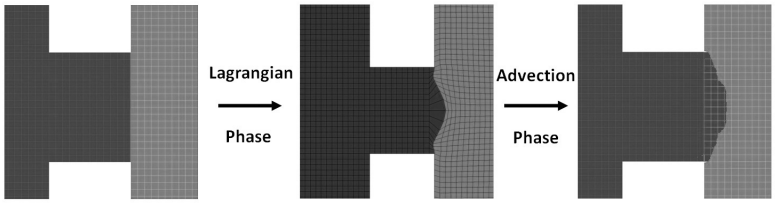

Fig. 1 Lagrangian and advection phases in one step.

$\overrightarrow{\psi}(\overrightarrow{\chi},t)$ that associates the ALE coordinates $\overrightarrow{\chi}$ in Ω_t^{ALE} at time t to the Eulerian coordinates $\overrightarrow{x}$ in Ω_t by:

$$\overrightarrow{x} = \overrightarrow{\psi}(\overrightarrow{\chi},t) \tag{2.1}$$

A description of the transformation of a material continuum body from the reference domain Ω_0 to the current domain Ω_t and ALE domain Ω_{ALE} is shown in Fig. 2. Let $f(\overrightarrow{x},t)$ be a function of the Eulerian coordinates $\overrightarrow{x}$ and the time t. The expression of $f(\overrightarrow{x},t)$ in the ALE referential is given by:

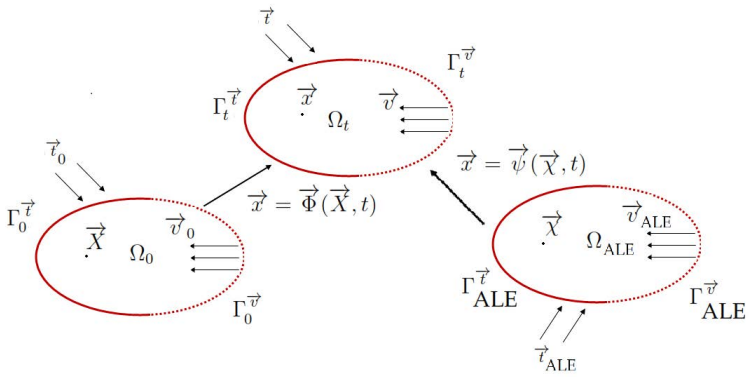

Fig. 2 Description of a material continuum body in the reference domain Ω_0, the current domain Ω_t and the arbitrary domain Ω_{ALE}

$$f(\vec{x},t) = f\left(\vec{\psi}(\vec{\chi},t),t\right) = f^{ALE}\left(\vec{\chi},t\right) \tag{2.2}$$

The partial time derivative of the function $f^{ALE}\left(\vec{\chi},t\right)$ in the ALE referential is given by:

$$\frac{\partial f^{ALE}\left(\vec{\chi},t\right)}{\partial t} = \frac{\partial f(\vec{x},t)}{\partial t} + \frac{\partial \vec{\psi}(\vec{\chi},t)}{\partial t}.\nabla_{\vec{x}} f(\vec{x},t), \tag{2.3}$$

where $\vec{v}_{ALE} = \frac{\partial \vec{\psi}(\vec{\chi},t)}{\partial t}$ is the ALE velocity.

Now, considering material time derivative is related to the partial time derivative by:

$$\frac{df(\vec{x},t)}{dt} = \frac{\partial f(\vec{x},t)}{\partial t} + \vec{v}.\nabla_{\vec{x}} f(\vec{x},t) \tag{2.4}$$

and subtracting Eq.2.3 from Eq.2.4, we finally obtain the relation between the material time derivative and the partial time derivative in the ALE referential:

$$\frac{df}{dt} = \frac{\partial f^{ALE}}{\partial t} + (\vec{v} - \vec{v}_{ALE}).\nabla_{\vec{x}} f \tag{2.5}$$

We denote by $\vec{w} = (\vec{v} - \vec{v}_{ALE})$ the convective velocity (difference between the fluid's velocity and the ALE domain velocity).

2.2 Conservation equations

The ALE formulation for the conservation equations is obtained by substituting the function $f(\vec{x},t)$ Eq.2.5 by the density, the velocity vector and the internal energy functions in the equations of the conservation of mass, conservation of linear momentum and conservation of energy, respectively. Thus, the ALE conservation equations are given by:

- **Conservation of mass**

$$\frac{\partial \rho}{\partial t} = -\rho\frac{\partial v_i}{\partial x_i} - w_i\frac{\partial \rho}{\partial x_i} \tag{2.6}$$

- **Conservation of linear momentum**

$$\rho\frac{\partial v_i}{\partial t} = \sigma_{ij,j} + \rho b_i - \rho w_i\frac{\partial v_i}{\partial x_j} \tag{2.7}$$

- **Conservation of energy**

$$\rho \frac{\partial E}{\partial t} = \sigma_{ij,j} v_{i,j} + \rho b_i v_i - \rho w_j \frac{\partial E}{\partial x_j} \tag{2.8}$$

There are two ways to implement the ALE equations; they correspond to the two approaches taken in implementing the Eulerian viewpoint in fluid mechanics. The first way solves the fully coupled equations for computational fluid mechanics; this approach, used by various authors can handle only a single material in an element as described for example in [4]. The alternative approach is referred to as an operator split, where the calculation for each time step is divided into two sequential phases (see [11]):

1. The Lagrangian phase, in which the mesh moves with the material; in this phase, the changes in velocity and internal energy due to the internal and external forces are calculated.
2. The advection phase is a mapping of the conservative variables (mass, momentum, and energy) from the deformed Lagrangian mesh into the arbitrary ALE new grid using re-meshing algorithms described in [12].

A shock viscosity with linear and quadratic terms derived by Von Neumann and Richtmeyer [13], is used to resolve the shock wave.

The solution is advanced in time using second-order time integration. Nodal displacements and velocities are updated as follows:

$$u^{n+\frac{1}{2}} = u^{n-\frac{1}{2}} + \Delta t . M^{-1} . (F_{ext} + F_{int}), \tag{2.9}$$

$$x^{n+1} = x^{n-1} + \Delta t . u^{n+\frac{1}{2}}, \tag{2.10}$$

where F_{int} is the internal vector force and F_{ext} the external vector force associated with body forces, coupling forces, and pressure boundary conditions, M is a diagonal lumped mass matrix.
The time step size Δt, is limited by the CFL stability condition (see [11]), which may be expressed as:

$$\Delta t \leq \frac{l}{c}, \tag{2.11}$$

where typically, l and c represent a characteristic length and a signal velocity (the speed of sound), respectively.

2.3 Euler-Lagrange fluid structure coupling

The Euler-Lagrange coupling is a method that combines the ALE multi-material formulation described in the previous subsection and the classical master-slave penalty contact method (see [14, 15]), commonly used to solve contact problems in solid mechanics. The Lagrangian structure is always the slave part and the Eulerian fluid the master part (see [16]).

In the Euler-Lagrange coupling, the structure is embedded in a Eulerian fixed mesh. This Eulerian fixed mesh will contain the Lagrangian structure and also the ALE fluid (single or multi-material) that flows through the mesh using an advection scheme to update the velocity and history variables.Since the fluid flows through a fixed mesh, there is no mesh distortion allowing the limitations of the constraint-based method due to great mesh deformation to be overcome(see [12, 14]). The Euler-Lagrange method also guarantees the conservation of momentum and energy, where constraint-based

method fails to conserve the total energy. The coupling forces between the fluid and the structure are similar to the contact forces and are defined by:

$$F = k.d, \tag{2.12}$$

where F is the force applied to both master and slave nodes in opposite directions, k is the contact stiffness, and d is a depth penetration that is incrementally updated at each time step. Indeed, if at time t^0 we have $d^0 = 0$, then, at time $t^{n+1} = t^n + \Delta t$, the penetration vector is updated by:

$$\overrightarrow{d}^{n+1} = \overrightarrow{d}^{n} + (\overrightarrow{v}_s - \overrightarrow{v}_f)\,\Delta t, \tag{2.13}$$

where $\overrightarrow{v}_s$ is the structure velocity at the slave node and $\overrightarrow{v}_f$ is the fluid velocity at the fluid node. A sketch of the coupling method is shown in Fig. 3.

There are many definitions for the stiffness, k; a good value of the stiffness should reduce the loss in energy conservation and prevent fluid leakage through the structure. In this study, the stiffness used is given in [17] and defined as:

$$k = p_f \frac{KA^2}{V}, \tag{2.14}$$

where K is the bulk modulus of the fluid element in the coupling that contains the slave node, V is the volume of the fluid element that contains the master node, A is the average area of the structure elements connected to the master node, and $0 \leq p_f \leq 1$ is a scalar factor introduced to avoid numerical instabilities.

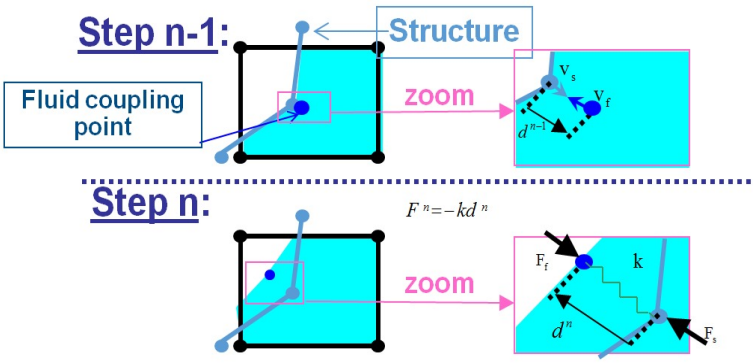

Fig. 3 Euler-Lagrange FSI coupling method in one step.

3 Shock tube experimental setup

3.1 Installation

The shock tube consists of two main parts: the driver section and the driven section (Fig. 4)[18, 19, 20]. The driver section contains compressed air, which is released into the driven section in order to create a shock wave. This is generally triggered with a burst plate or high speed valve. In the given experiments, a shock wave is generated in water by releasing high pressure air through a high-speed valve. The shock wave propagates through water in the driven section [18, 19, 20]. At the end of

the driven section, a T-section is fitted, enabling the secure mounting of a test specimen. The test specimen is mounted with a rosette strain gauge in order to capture the strains created by the shock wave impact.

In these experiments, three pressure sensors (one static and two piezoelectric sensors) are placed at three different locations (sensors boss 1, boss2 and boss 3 in Fig. 4) in the shock tube to capture the propagation of the shock wave.

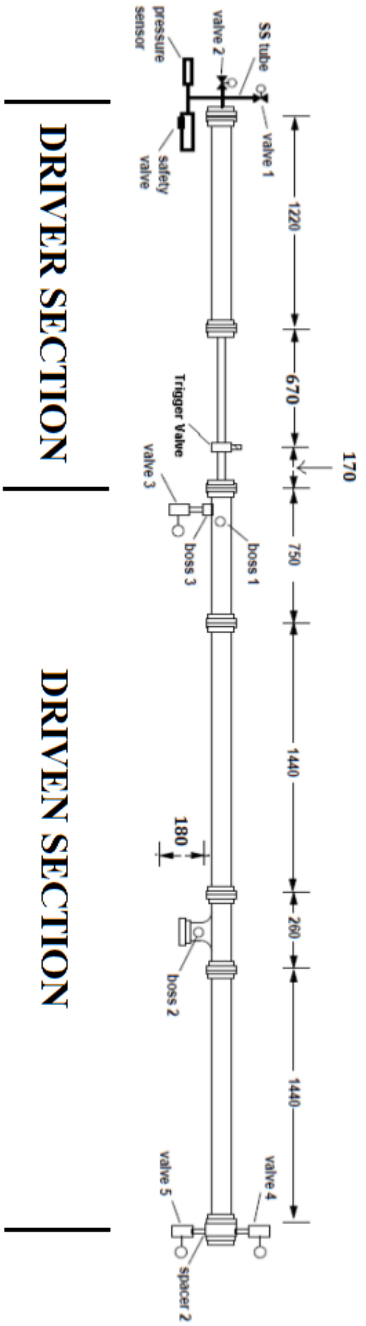

Fig. 4 Shock Tube Fabrication details diagram (dimension in mm)

3.2 Experimental results

Several experiments were performed and it was found that the strain profile is a linear mapping of the driven pressure profile (see Fig. 5).
In order to validate the results, the experiments were also repeated on the same test piece. Repeated experiments proved that CFRP test pieces can withstand shock pressure. However, it is worth noting that applied shock pressure in these experiments did not result in strains for more than 25% of the strain limit for rupture. It can be deduced that the material behaves linearly under shock pressure.

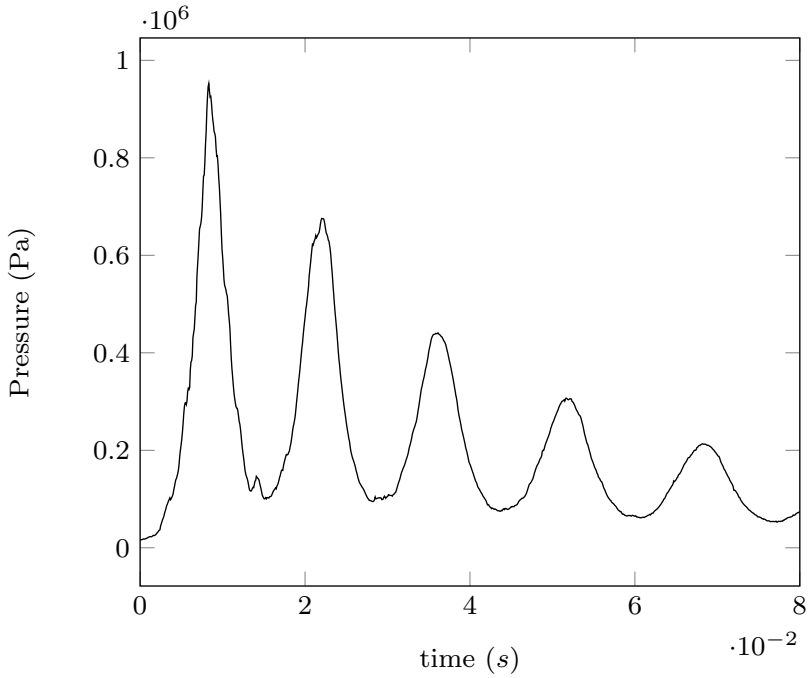

Fig. 5 Driven pressure profile in shock tube at the pipe T-section junction.[18]

4 Shock tube numerical setup

In this work, multiphysics numerical analysis was carried out on a CFRP test piece subjected to a shock wave attached to a tube. This setup has been commonly used to test material under dynamic loading [18]. In the previous work [18, 21], FSI effects were not considered and were lacking in the total response of the structures, since the water in the tube dampens the CFRP displacement when it goes into its vibration mode exposed to the cyclic pressure loading.

To complete the previous work, the T-section of the shock tube, including the water contained inside the tube and the test piece, are modeled using LS-DYNA® commercial package. The simulation starts when the shock wave reaches the entrance of the section; the time history of the pressure recorded by the experimental setup is set as an input pressure (in the green FEM elements in Fig. 6). Here, the physics of the shock wave in the fluid mediums and the composite shell material were

strongly coupled using the advanced Euler-Lagrange fluid-structure interaction (FSI) technique, previously described. The pipe walls are stiff enough to not consider the FSI effects between the water and the stiff pipe. However, due to the fluid's viscosity and the effects at the boundary, stick boundary conditions are used at the fluid pipe interface by constraining the fluid's velocity to be zero in order to model the friction at the pipe's wall. A sketch of the testing section describes the fluid structure interface in Fig. 6.

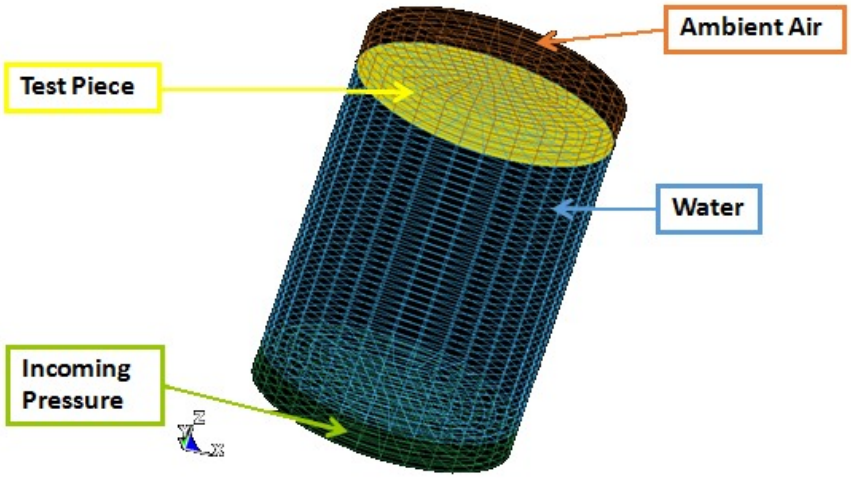

Fig. 6 Testing section FSI model; Green mesh shows the connection between the T-section and the rest of the shock tube, blue mesh shows the water section, yellow shows the composite shell elements, and brown mesh shows the atmospheric air.

4.1 Fluid constitutive material models:

For both fluids (water and air), the same constitutive fluid material model is used, as shown:

$$\sigma = -P.I_d + \tau \tag{4.1}$$

where $\sigma, -P.I_d, \tau = 2\mu\dot{\varepsilon}, \mu$ denotes the stress tensor, its normal and deviatoric components, the dynamic viscosity and the strain rate, respectively.

The pressure term for air is calculated with the classical ideal gas law equation of state ($\gamma = 1.4$). The pressure term of the water is calculated using the barotropic $u_s - u_p$ Mie-Gruneisen law, given by:

$$P = \frac{\rho_0 c^2 \nu(1+\nu)}{(1-(s-1)\nu)^2} \tag{4.2}$$

where P, ρ_0, c and ν are, respectively, the pressure, the nominal density, the speed of sound and the specific relative volume, s is the slope of the Hugoniot shock curve [22], where u_s and u_p are the shock and the particle velocities, respectively.

4.2 CFRP shell constitutive material model:

The carbon fiber reinforced polymers (CFRP) quasi-isotropic shell structure is modeled by a linear isotropic material. The homogenization strategy was proposed by the co-authors, with the input material model parameters being obtained by experimental MTS® study [18]. Validation of the homogenized parameters for the numerical study has also been provided in [18] against experimental data using the commercial FEM code ANSYS [23]. The same equations and parameters were used in this paper to simulate the dynamic behavior of the composite shell CFRP subjected to water shock waves.

Material	Density $(kg.m^{-3})$	Dynamic Viscosity
Air	1.28	$1.983e^{-5}$
Water	998	$1e^{-3}$

Table 1 Fluid's material model parameters

Material	s	Speed of sound $c(m.s^{-1})$	$V0 = \frac{1}{1+v}$
Water	1.9	1480	0.999954272

Table 2 Mie-Gruneisen equation of state

Material (Homog.)	Density $(kg.m^{-3})$	Young's Modulus (Pa)	Poisson ratio
CFRP	1760	$2.6751e^{10}$	0.2

Table 3 Composite shell's material model parameters

5 Comparison between experimental and numerical results

The shock tube was modeled using the ALE method, where equations of state were solved for the two fluids to capture the physics. The shock wave was generated by the interaction of high-pressure air with water at atmospheric pressure. The generated hock wave, propagates along the T-section filled with water and impacts the CFRP test piece, as shown in Fig. 7 and Fig. 8.
Experimental and numerical results are compared in terms of X-strain at the location of the strain gauges: at the top of the composite shell (outward normal pointing to the ambient air) in its center. The comparison between uncoupled and coupled numerical solutions is shown in Fig. 9, while the comparison between strongly coupled numerical simulation with FSI and experimental results is shown in Fig. 10.
The mean strain results are found to be in reasonable agreement with the experimental data (Fig. 9). However, we can clearly see that there are oscillations in the strains data (Fig. 9 and Fig. 10). The oscillation frequencies in the strain data with FSI is lower than without FSI, which is due to the fact

that added water mass causes damping.
The Power Spectral Density (PSD), normalized by its maximum amplitude and both X-strain results (with and without FSI) are shown in Fig. 11. We observe that the input pressure loading frequency is in the range of 80 - 100Hz and well captured for both simulations. FSI strains results have oscillation frequencies in the range of 400-600 Hz whereas these values are extraordinarily high (1500-1800 Hz) in strains without FSI.

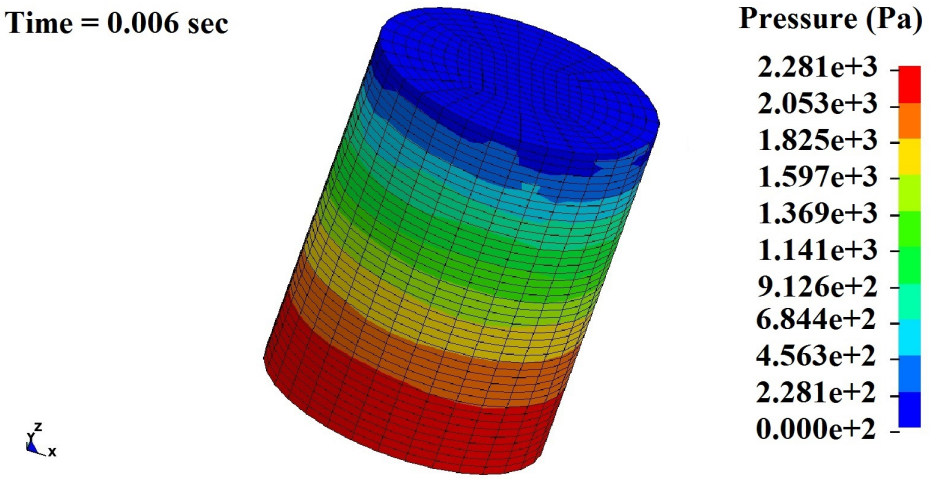

Fig. 7 Visualization of translation of pressure shock front (in Pascal) in shock tube T-section at time $t \approx 6ms$.

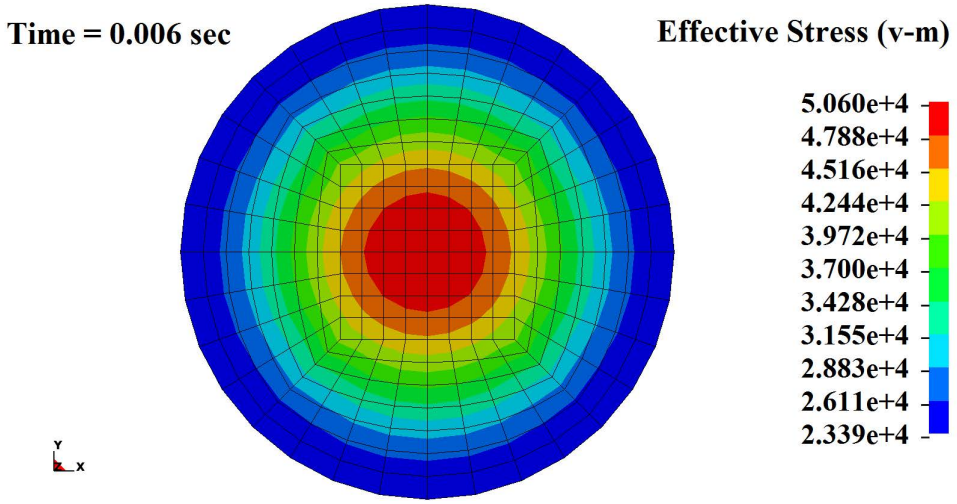

Fig. 8 Visualization of the CFRP shell Von-Mises stresses at time $t \approx 6ms$.

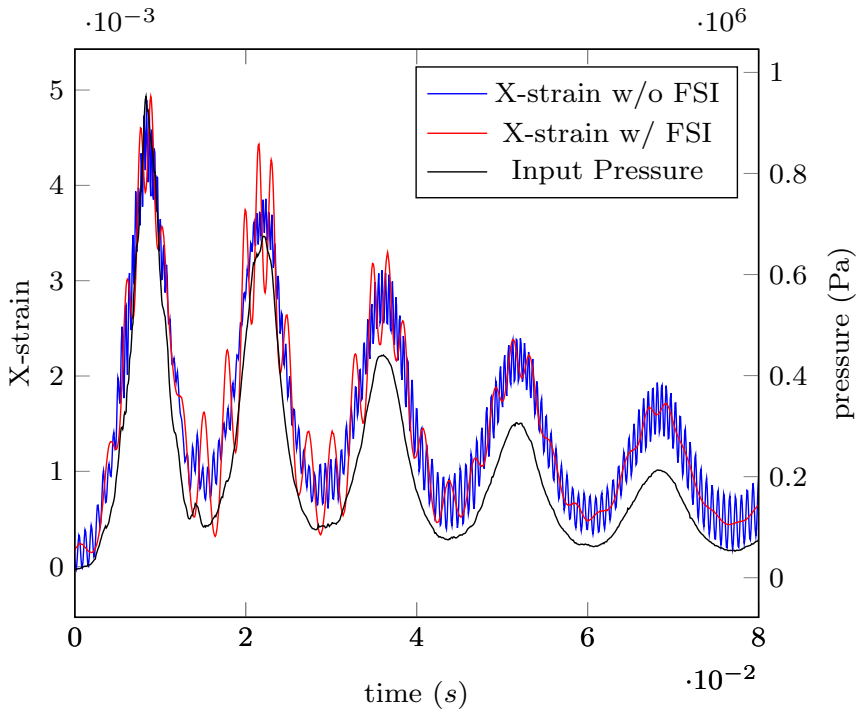

Fig. 9 Comparison between numerical X-strain results, with FSI (in red) and without FSI (in blue), taken at the top of the composite shell at its center; input pressure obtained from experimental tests is plotted in black.

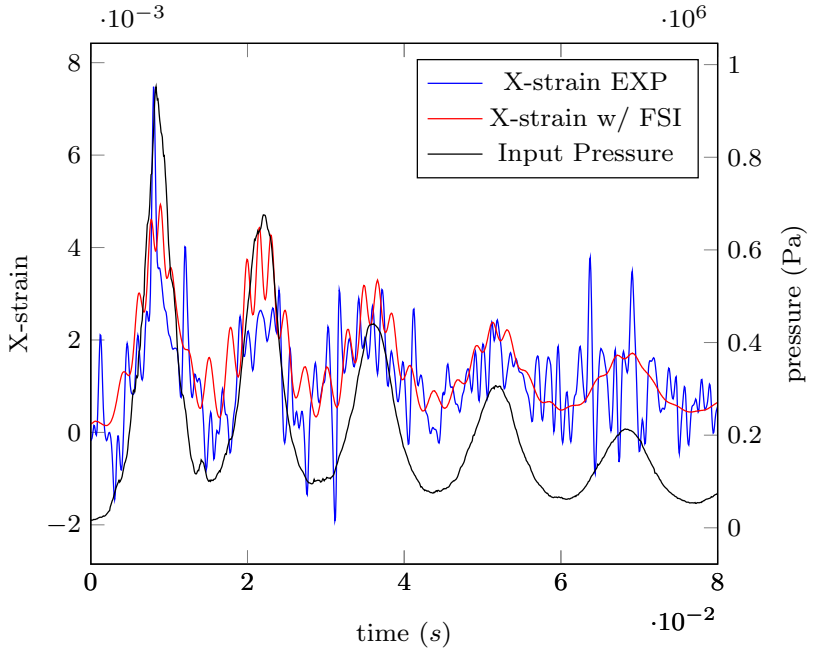

Fig. 10 Comparison between numerical with FSI (in red) and experimental (in blue) X-strain results taken at the top of the composite shell at its center. Input Pressure obtained from experimental tests is plotted in black.

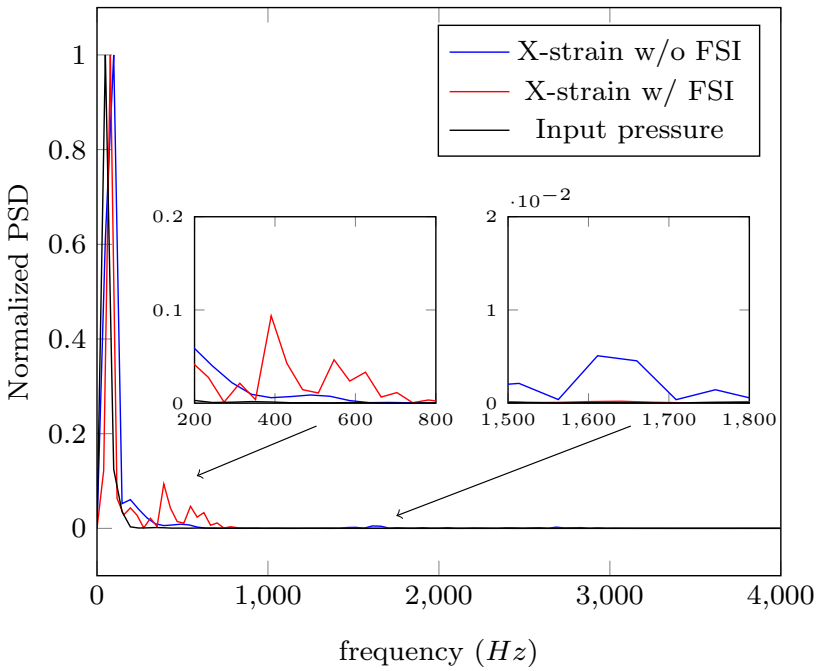

Fig. 11 Power spectral density (PSD) normalized by its maximum amplitude of the X-Strain results without FSI (blue) and with FSI (red), and the input pressure (in black).

6 Conclusion

Results from the shock tube experimental setup and the numerical simulations using LS-DYNA® proved that, under dynamic loading, CFRP E720 composite behaves linearly. Good agreement between strongly coupled simulations and experimental results confirms that the FSI capabilities of LS-DYNA® can be used for the modeling of deforming structures under dynamic loading, especially in the case discussed.
Once numerical is validated with experimental test results, several simulations can be performed for the improvement of final prototypes and used by design engineers in different industries (see [24]) for the purpose of minimizing both cost and time consumption.

7 Acknowledgements

The authors acknowledge the Norwegian Research Council for sponsoring this project under PETROMAKS grant no 200585. The authors would also like to acknowledge the support of Linda March from The Good English Company, UK for proofreading this work.

References

[1] N. Aquelet, M. Souli, and L. Olovsson. Eulerlagrange coupling with damping effects: Application to slamming problems. *Computer Methods in Applied Mechanics and Engineering*, 195(1-3):110–132, 2005.

[2] Hassan a; Khawaja, Ramzi Messahel, Bruce Ewan, Mhamed Souli, and Mojtaba Moatamedi. Experimental and Numerical Study of Pressure in a Shock Tube. *Journal of Pressure Vessel Technology*, 138(4):041301, 2016.

[3] M. U. Khan, M. Moatamedi, M. Souli, and T. Zeguer. Multiphysics out of position airbag simulation. *International Journal of Crashworthiness*, 13(2):159–166, 2008.

[4] Z. Ozdemir, Y.M. Fahjan, and M. Souli. Numerical evaluation of nonlinear response of broad cylindrical steel tanks under multidimensional earthquake motion. *Earthquake Spectra*, 28(1):217–238, 2012.

[5] M. Souli, A. V. Kulstep, E. A. Al-Bahkali, C. C. Pain, and M. Moatamedi. Arbitrary lagrangian eulerian formulation for sloshing tank analysis in nuclear engineering. *Nuclear Science and Engineering*, 183(1):126–134, 2016.

[6] R. Messahel, B. Cohen, M. Souli, and M. Moatammed. Fluid-structure interaction for water hammers effects in petroleum and nuclear plants. *The International Journal of Multiphysics*, 5(4):377–386, 2011.

[7] R. Messahel, B. Cohen, M. Moatamedi, A. Boudlal, M. Souli, and N. Aquelet. Numerical and experimental investigations of water hammers in nuclear industry. *The International Journal of Multiphysics*, 9(1):21–36, 2015.

[8] M. Moatamedi, M. Souli, and E. A. Al-Bahkali. Fluid structure modelling of blood flow in vessels. *Molecular and Cellular Biomechanics*, 2014.

[9] M. Souli, E. A. Al-Bahkali, T. Al-Bahkali, and M. Moatamedi. Investigation of blood flow modeling in artery using ale formulation. *The International Journal of Computational Methods*, 2016.

[10] M. Souli and F. Erchiqui. Experimental and numerical investigation of instructions for hyper-elastic membrane inflation using fluid structure coupling. *Computer Modeling in Engineering and Sciences*, 77(3):183–200, 2011.

[11] D.J. Benson. Computational methods in lagrangian and eulerian hydrocodes. *Computer Methods in Applied Mechanics and Engineering*, 99(2-3):235–394, 1992.

[12] J.O. Hallquist. Ls-dyna theory manual. *Livermore Software Technology Corporation*, 1998.

[13] J. Von Neumann and R.D. Richtmeyer. A method for the numerical calculation of hydrodynamical shocks. *Journal of Applied Physics*, 21:232–257, 1950.

[14] Z. Sun, D. Howard, and M. Moatamedi. Application of the penalty coupling method for the analysis of blood vessels. *European Journal of Computational Mechanics*, 16(3–4):537–548, 2007.

[15] I. Pericevic and M. Moatamedi. Finite element analysis of footwear and ground interaction. *Strain*, 41(3):113–115, 2005.

[16] M. Souli and D.J. Benson. Arbitrary lagrangian eulerian and fluid-structure interaction: Numerical simulation. *Wiley-ISTE*, 2010.

[17] Z.H. Zhong. Finite element procedures for contact-impact problems. *Oxford Science Publications*, 1993.

[18] H.A. Khawaja, T.A. Bertelsen, R. Andreassen, and M. Moatamedi. Study of cfrp shell structures under dynamic loading in shock tube setup. *Journal of Structures*, 2014.

[19] H. Ji, M. Mustafa, H.A. Khawaja, E.C. Bruce, and M. Moatamedi. Design of water shock tube for testing shell materials. *World Journal of Engineering*, 11(1):50–60, 2014.

[20] H.A. Khawaja, J. Kapaya, and M. Moatamedi. Shock tube detail overview of equipment and instruments in the shock tube experimental setup. *Lambert Academic Publishing*, 2015.

[21] H.A. Khawaja and M. Moatamedi. Multiphysics investigation of composite shell structures subjected to water shock wave impact in petroleum industry. *Materials Science Forum*, 2013.
[22] S.P. Marsh. Lasl shock hugoniot data. *University of California Press*, 5, 1980.
[23] ANSYS. Theory reference, in structures, static analysis. *Academic Research*, release 14.0, 2014.
[24] W. L. Cheng, S. Itoh, K.C. Jen, and M. Moatamedi. A new analytical model for high-velocity impact of thick composites. *International Journal of Crashworthiness*, 12(1):57–65, 2007.